Brittle versus ductile deformation as the main control of the deep fluid circulation in oceanic crust

Marie Violay, Benoit Gibert, David Mainprice, Jean-Pierre Burg

AGU PUBLICATIONS

Geophysical Research Letters

RESEARCH LETTER
10.1002/2015GL063437

Key Points:
- Basalts are brittle and dilatant up to 800°C
- At temperature > 800°C basalts are ductile and compacting
- The BDT may be considered as a limit of permeability in the oceanic crust

Correspondence to:
M. Violay,
marie.violay@erdw.ethz.ch

Citation:
Violay, M., B. Gibert, D. Mainprice, and J.-P. Burg (2015), Brittle versus ductile deformation as the main control of the deep fluid circulation in oceanic crust, *Geophys. Res. Lett.*, *42*, 2767–2773, doi:10.1002/2015GL063437.

Received 12 FEB 2015
Accepted 26 MAR 2015
Accepted article online 27 MAR 2015
Published online 24 APR 2015

Brittle versus ductile deformation as the main control of the deep fluid circulation in oceanic crust

M. Violay[1], B. Gibert[2], D. Mainprice[2], and J.-P. Burg[1]

[1]D-ERDW, ETH, Zürich, Switzerland, [2]Geosciences Montpellier, Université de Montpellier-CC060, Montpellier, France

Abstract The brittle to ductile transition may strongly influence hydraulic properties of rocks at the depth and temperature ranges that hydrothermal fluids circulate. To examine this transition in the context of the oceanic crust, we conducted a series of deformation experiments on a natural basalt sample at in situ oceanic crust conditions. Dilatancy was measured during deformation. The method consisted in monitoring the volume of pore fluid that flows into or out of the sample at constant pore pressure. Mechanical and microstructural observations at experimental constant strain rate of 10^{-5} s^{-1} indicated that the basalt was brittle and dilatant up to 800°C. At higher temperature, the deformation mode became macroscopically ductile and samples compacted. These observations have important implications on heat transfer and fluid migration in oceanic crust.

1. Introduction

The mid-ocean ridge system is the largest continuous volcanic feature on Earth, with significant interactions between tectonic activity, volcanism, and seawater circulation [*Macdonald*, 1982]. At mid-ocean ridges, new crust is formed and cools by heat conduction and hydrothermal circulation [e.g., *Johnson et al.*, 1993; *Morgan and Chen*, 1993; *Stein and Stein*, 1994]. The decline of permeability across the brittle-ductile transition (BDT) is the main factor controlling the heat and fluid transfer from magmatic chamber to hydrothermal systems [*Hayba and Ingebritsen*, 1997; *Driesner and Geiger*, 2007; *Weis et al.*, 2012]. Indeed, it is generally thought that the magma chamber is surrounded by a hot and ductile carapace through which heat transfer is conductive because the plastic behavior of the rock will close possible fluid pathways [*Rojstaczer et al.*, 2008]. Farther outward, as temperature declines, the rock will encounter the BDT with a concomitant increase in permeability [*Fournier*, 1999]. The thickness of the conduction-dominated, ductile boundary zone between magma and the circulating fluid directly determines the rate of heat transfer. The dependence of permeability on the temperature-dependent mechanical rock properties controls how fast and to what temperatures the circulating fluids can extract heat. There are some economic uses of hydrothermal circulation, as, for example, geothermal power [e.g., *Palmason*, 1974; *Asmundsson et al.*, 2014] and mining ore deposits in extinct fluid pathways [*Nelson and Giles*, 1985; *Mills and Elderfield*, 1995]. Our current understanding of hydrothermal circulation around the BDT at mid-ocean ridge has been aided by geophysical observations. On the one hand, heat flux measurements and seismic studies show that hydrothermal circulation up to 700°C should be taken into account to explain cooling of the oceanic crust [*Sleep and Rosendahl*, 1979; *Chen and Morgan*, 1990; *Morgan and Chen*, 1993; *Stein and Stein*, 1994; *Fontaine et al.*, 2001, 2008]. On the other hand, the hydrothermal circulation around the BDT is ill constrained due the limited number of in situ porosity and permeability measurements. Indeed, such measurements are rare at depths > 2–3 km, and there are none deeper than approximately 10 km [*Ingebritsen and Manning*, 2010]. Moreover, experimental determination of porosity and permeability of low-porosity rocks at temperature and pressure representative of the BDT has received remarkably little attention in the literature. Existing laboratory measurements indicate that dilatancy (porosity increasing with strain) and permeability increase for both brittle failure and cataclastic flow. Permeability often decreases during the initial crack closure stage and then increases at the onset of dilatational microcracking until localized brittle failure occurs [*Zoback and Byerlee*, 1975; *Peach and Spiers*, 1996; *Zhu and Wong*, 1997; *Mitchell and Faulkner*, 2008; *De Paola et al.*, 2009]. In the ductile domain, low-porosity rocks can be associated with minor dilatancy or compaction depending of the deformation mechanism. For the cataclastic creep mechanism in calcite [*Zhang et al.*, 1994], in quartz-calcite aggregate [*Siddiqi et al.*, 1997], and in anhydrite [*De Paola et al.*, 2009], ductile deformation is associated with minor dilatancy that

leads to a small increase in permeability with increasing strain, until it is stabilized at a percolation threshold. For other deformation mechanisms such as hydrostatic compaction [*Bernabé et al.*, 1982] and shear-enhanced compaction [*Zhang et al.*, 1994], ductile deformation can decrease the pore space and reduce the permeability. Little is known regarding the effect on fluid-transport properties in rocks undergoing ductile deformation by crystal plastic or diffusion flow mechanisms (but see *Fischer and Paterson* [1989]). When rocks are deformed in triaxial configuration at elevated temperatures and large effective pressures, permeability and porosity tend to be reduced with strain, although the response depends critically on the state of drainage of the pore fluid [*Fischer and Paterson*, 1989, 1992].

Until now, technical challenges related to pore fluid confinement impeded investigating the porosity evolution in experiments that reproduce deformation conditions typical of the brittle to ductile transition in basalt oceanic crust [*Violay et al.*, 2012]. We surpassed this limitation thanks to the technical improvements of the Paterson apparatus at the Rock deformation laboratory of ETH Zurich, equipped with a purpose-built pore pressure system. This allowed us to measure porosity and rheological properties of basalt at oceanic in situ crustal pressure-temperature (*P-T*) conditions, i.e., at confining pressure of 130 MPa equivalent to a depth of 4–5 km, temperatures from 600°C to 1050°C, and pore fluid pressure of 30 MPa. The results will improve our ability to analyze heat transfer between magmatic intrusions and high-enthalpy hydrogeothermal systems, to model the migration of fluids through nominally ductile crust beneath volcanoes and, more generally, will aid in understanding the nature of permeability as a function of depth in the oceanic crust.

2. Methods

2.1. Experimental Method

2.1.1. Triaxial Deformation Experiments

Cylindrical samples of 10 mm in diameter and 20 mm in length were jacketed with copper or iron after being dried over 48 h at 70°C. To reduce jacket strength, copper was used at low temperatures (600 to 750°C), whereas iron jackets were used above that range. These assemblies were then deformed in conventional triaxial experiments conducted in a servo-controlled, gas-medium apparatus from "Paterson instruments." Temperatures ranged from 600°C to 1050°C; confining pressure (P_c) and pore pressure (P_p) were held constant at 130 and 30 MPa, respectively, yielding an effective confining pressure (P_c^{eff}) of 100 MPa. Argon was used as pore fluid. Deformation experiments were generally performed up to strains of 10% with constant axial strain rate ($\dot{\varepsilon}$) of $10^{-5}\,s^{-1}$. The nominal strain rate of $10^{-5}\,s^{-1}$ was sufficiently slow to ensure a fully "drained" condition [*Fischer and Paterson*, 1989]. In effect, argon diffusion in the sample requires a minimum time scale given by [*Fischer and Paterson*, 1989]: $t = l^2 \cdot \eta \cdot \beta/\kappa$, with l: the specimen length, η: the dynamic viscosity of the fluid, β: the storage capacity per unit volume, and κ: the permeability. Taking $\eta = 10^{-4}$ Pa s for argon at experimental temperature and pressure, $l = 10$ mm, and $\kappa/\beta = 10^{-11}$ Pa m^2 (for the lowest permeability measured ($\kappa = 10^{-19}$ m^2), $t \sim 1000$ s). This minimum time scale is of the same order as the time required for 1% axial strain at strain rate of $10^{-5}\,s^{-1}$ (considering that dilatation is due to ~1% axial strain).

Differential stresses were measured with both an internal and external load cell, with an accuracy of 2 MPa. Corrections were applied to the measured force with jacket strengths estimated from *Frost and Ashby* [1982] and from the change in sample dimensions with deformation; displacement measurements were corrected for apparatus distortion.

2.1.2. Volume Change

The apparatus was equipped with a pore fluid volumometer and upstream and downstream pore fluid connections (Figure 1). The volumometer can be used in conjunction with axial testing, or under hydrostatic conditions, and thus allowed the generation of a pore pressure (argon gas), measurement of permeability (by transient flow method), and pore fluid volume changes during deformation. However, the long time required to measure the permeability by the transient flow method, associated with sample mechanical relaxation, and sample porosity healing at high temperature, impeded measuring accurately the permeability during deformation.

The volumometer was fitted with displacement and pressure transducers located in such a way as to minimize any "dead" volume. Pore pressure was measured with an accuracy of 0.1 MPa. The volumometer piston displacement was measured with a Schaevitz linear voltage differential transducer (LVDT) located

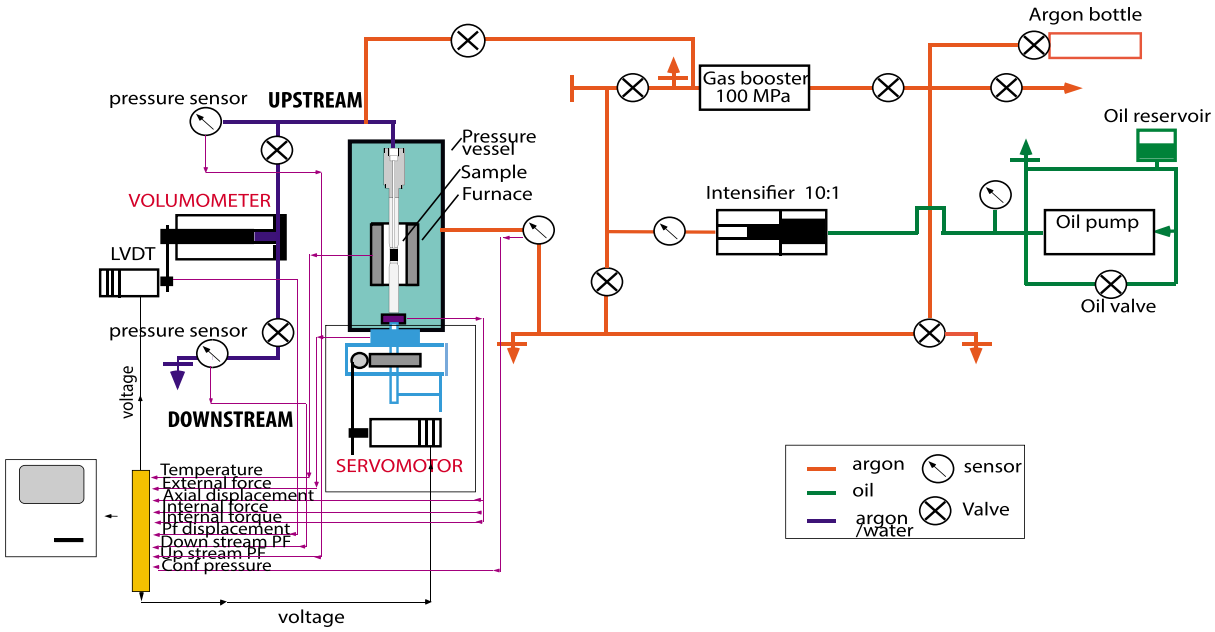

Figure 1. Schematic diagram of the experimental apparatus. Dilatancy was measured during constant strain rate axial deformation.

within the ball screw, on the axis of the actuator, and had a resolution of 0.01 mm. The volumometer piston was precisely 7 mm in diameter, with 50 mm stroke. Volume change during deformation was calculated from the changes in output of the LVDT. The calculated volume was first corrected for possible small leaks and apparatus distortion (i.e., volume changes associated with the elastic distortion of the pore fluid system during loading, as determined with an impermeable sample); in temperature experiments, the temperature gradient in the connecting pipes was assumed to remain constant during experiments. Correction was made for the difference in temperature between the sample and the volumometer by multiplying the ratio of the molar volumes of argon at high temperature and room temperature. The ratios were derived from *Fischer and Paterson* [1989]. This allowed measuring dilatancy or compaction during deformation (i.e., inelastic volume change relative to axial strain). As example, the variation of porosity during deformation of sample GFB 15 is displayed Figure 2.

2.1.3. Experimental Procedure

The procedure for the triaxial experiments consisted in the following steps: (1) first, the confining pressure was raised to 30 MPa. (2) Then the argon pore fluid was introduced at pressure 10 MPa by drawing argon from the confining pressure system (i.e., from orange line to blue line in Figure 1). This pore pressure was maintained for 24 h or longer to insure complete saturation of the sample. (3) Then, the confining pressure and the pore pressure were both increased simultaneously to the target pore pressure (4) once the targeted pore pressure was achieved, the confining pressure was further increased to apply the targeted effective confining pressure, (5) then the sample was heated at a rate of 20°C/min while the confining and pore pressures were adjusted, and (6) finally, an axial strain rate was imposed on the sample while the pore pressure was maintained constant at 30 MPa during experiments by a set-point controller connected to the servomotor driving volumometer piston.

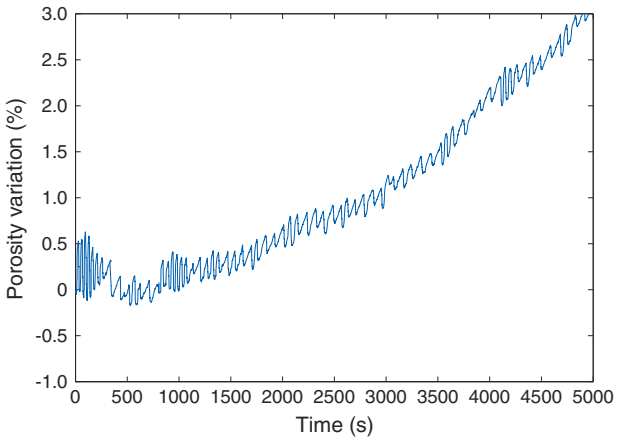

Figure 2. Porosity variation versus time at confining pressure of 130 MPa, pore fluid pressure of 30 MPa, and temperature of 650°C.

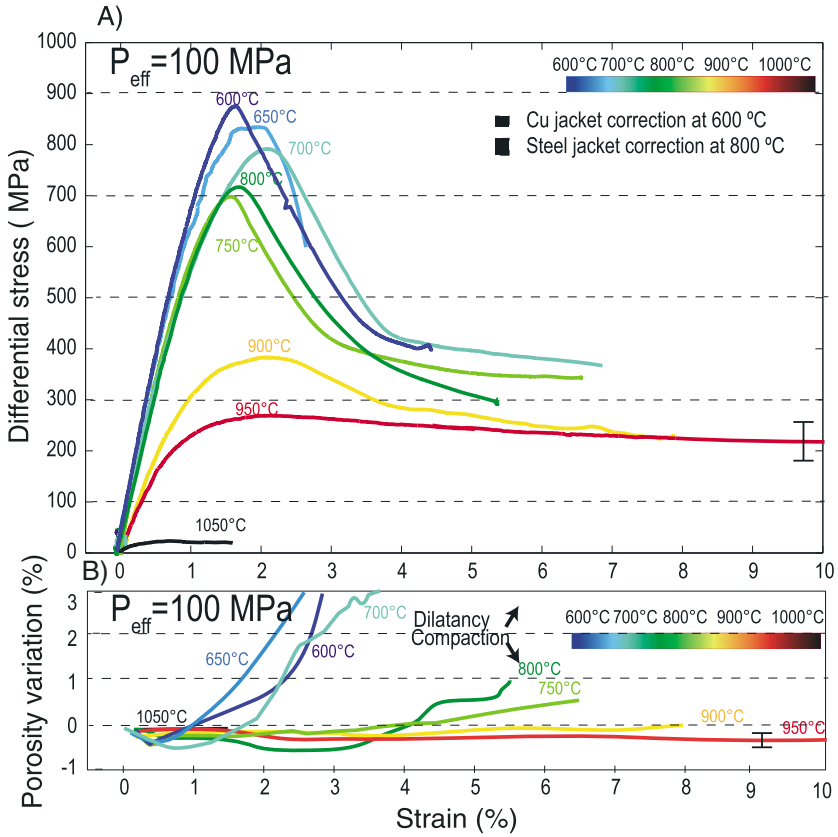

Figure 3. Differential stress and porosity variation versus strain curves for experiments conducted at temperature between 600 and 1050°C and confining pressure of 130 MPa. Pore fluid pressure (argon) was maintained at 30 MPa. The initial strain rate for all experiments was 10^{-5} s^{-1}. Correction for jacket contribution to mechanical strength is used for copper jacket at 600°C and iron jacket at 800°C.

2.2. Starting Material

The samples were taken from columnar basalts in the Escandorgue flow, Languedoc-Roussillon, France. Samples were selected for their low porosity <2.7% (measured with a pycnometer), their low degree of alteration, and simple mineralogical composition [*Violay et al.*, 2012]. These microcrystalline to cryptocrystalline basalts contain approximately 5 vol % of phenocrysts (essentially clinopyroxenes and a few olivines). The fine-grained groundmass is a homogeneous mixture of plagioclase (35–45 vol % of the total rock), clinopyroxene (25–35%), feldspathoids (10%), and titanomagnetite (5–15%). Olivine phenocrysts are subhedral, equant glomerocrysts of fosterite (Fo79), about 300 μm in diameter. Clinopyroxene phenocrysts are subhedral laths or prisms of augite, about 100 μm long; compositional zoning of titanium is common. Clinopyroxene crystals in the groundmass (grain size ~10–100 μm) are slightly more titaniferous than clinopyroxene phenocrysts (grain size ~ 200–500 μm). Groundmass plagioclases are subhedral laths with composition varying from labradorite to oligoclase. The feldspathoids are euhedral laths of leucite and nepheline, averaging 50 μm in length. Over scales less than 1 mm, there is local preferred orientation of the feldspathoid and plagioclase crystals, probably due to magmatic flow. Thermogravimetric measurements up to 1200°C showed that the GFB samples do not contain volatiles.

2.3. Analytical Method

After deformation, samples were impregnated with epoxy and then cut parallel to the cylinder axis, or, if deformation was localized, perpendicular to the shear plane. From each sample, a polished, 30 μm thin section was prepared and examined in an optical microscope using plane-polarized, cross-polarized and reflected light, and in a scanning electron microscope.

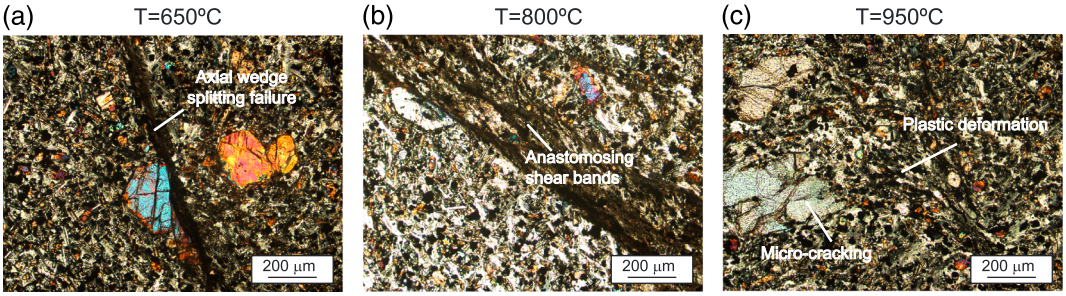

Figure 4. Photographs of jacketed samples deformed at different temperatures of (a) 650°C, (b) 800°C, and (c) 950°C. Optical plane-polarized light micrograph.

3. Results

3.1. Mechanical Data and Volume Changes

We conducted eight triaxial deformation experiments at 130 MPa confining pressure, 30 MPa pore fluid pressure, strain rate of $10^{-5}\,s^{-1}$, and temperature from 600°C to 1050°C (Figure 3).

Elastic behavior at very low strains was followed by one of three deformation modes, depending on temperature. Between 600 and 700°C, samples yielded at ~400 MPa and then rapidly hardened to peak stress that depended directly on temperature. Peak strength was systematically followed by strain weakening up to strains of about 3–7%. Volume changes were recorded over the whole temperature range. A notable feature was the tendency for compaction to occur at small strain (<1%), followed by important dilatation at larger strains.

At intermediate temperatures, 750 to 800°C, samples yield at 350 MPa. Peak stress was systematically followed by strain weakening up to strains of about 5–7%. Volume changes were recorded with a tendency for compaction at strain up to 3%, followed by small dilatation (up to 1% porosity) at larger strain.

At the highest temperature range, from 900 to 1050°C, the peak strength decreased with temperature and was followed by modest, monotonic weakening. Volume changes were very small, with a linear tendency for compaction at all strains.

3.2. Deformation Textures and Microstructures

At 600–700°C, and at strain comprised between 4% and 10%, strain was localized, often along a main fault associated with smaller subparallel or intersecting cracks and faults. At low temperatures (100 MPa, 600, and 650°C), the sample failed by axial wedge splitting (Figure 4).

At $700 < T < 800$°C, anastomosing, approximately 100 to 500 μm thick shear bands developed. Their bulk thickness increased with temperature. These shear zones were inclined 30° to 45° to the compression direction (i.e., parallel to the cylinder axis) and contained brittle cataclastic microstructures (microcracks and gouge). The angular fragments in the shear zones are between 0.01 μm and 10 μm in size, reduced from the initial phenocrystal size of 100–500 μm.

At intermediate $800 < T < 900$°C, the sample deformed by a combination of diffuse microcracking, mostly inclined 40° to 50° to the compression direction and plastic deformation of the minerals (Figure 4c).

At temperatures > 950°C, deformation was macroscopically homogeneously distributed. But, even at the highest temperatures, the indications of intracrystalline deformation are rare (except for titanomagnetite that shows plastic elongation). Microstructures are consistent with those reported in *Violay et al.* [2012], over the whole temperature range (Figure 4).

4. Discussion

4.1. Brittle to Ductile Transition and Porosity Evolution

The new mechanical data and microstructural observations show brittle failure and stress drops of basalt at temperatures from 600 to 850°C (at $P_c^{eff} = 100$ MPa, and $\dot{\varepsilon} = 10^{-5}\,s^{-1}$). Deformation is localized along discrete

fracture zones with the development of a thin and fine-grained coating of gouge. Porosity began decreasing during deformation, which is interpreted as closure of initial cracks within the sample. Then, porosity increased exponentially up to the yielding stress. This porosity increase is interpreted as the development of intragranular cracks [*Zoback and Byerlee*, 1975; *Zhang et al*., 1994; *Peach and Spiers*, 1996; *Zhu and Wong*, 1997, 1999; *Mitchell and Faulkner*, 2008]. Finally, porosity increased dramatically during failure, especially for experiments between 600 and 700°C. These variations are comparable to porosity changes previously reported on very low porosity rocks (e.g., *Fischer and Paterson* [1989], on Carrara marble). At temperatures from 850 to 1050°C, deformation was distributed and accommodated by intragranular microcracks and local crystal plasticity (Figure 4c). The lack of localized faulting under these conditions denotes ductile deformation in the sense of *Paterson and Wong* [2005], which corresponds to a macroscopic characterization of the aggregate deformation, as are stress-strain and porosity measurements. The evolution of porosity during ductile deformation was relatively simple, with a linear and very small decrease with increasing axial strain. This is interpreted in terms of collapse of initial porosity by crystal plastic or diffusional flow and change in porosity connectivity [*Fischer and Paterson*, 1989]. Because, the time for argon diffusion in the specimen is comparable to that for ~1% axial deformation (see method), a lag in the detection of dilation in the course of deformation may exist in experiments at $>$ 800°C (i.e., very low permeability).

4.2. Implications and Applications

The BDT in rocks has often been described as a parameter that may influence permeability and the porosity topology. However, experimental evidence for very low porosity magmatic rocks was lacking so far. This work shows that the BDT was associated with a transition from dilatant to compacting behavior in basalt. Previous experimental work by *Violay et al*. [2012] (performed on the same basalt used in this work) showed that extrapolation of the mechanical data to natural strain rate of $10^{-14}\,s^{-1}$ places the BDT in Icelandic crust near the isotherm 550 ± 100°C. Based on this assumption and considering the temperature gradients in volcanic zones in Iceland (~100°C/km), the presented experiments indicate that hydrothermal fluids might circulate, at least transiently, through the oceanic basaltic crust down to 4 to 6 km depth. This estimate is consistent with the lower limit of the Icelandic seismogenic zone, which is associated with the 650 ± 100°C isotherm [*Fridleifsson and Elders*, 2005]. At these depths and temperatures, fluids are supercritical. Such fluids have been recently recognized to be of important scientific and industrial interest, in particular for geothermal energy. *Fridleifsson and Elders* [2005] and *Friðleifsson et al*. [2014] predict that the extraction of supercritical fluids may enhance by a factor of 10 the electrical power of conventional geothermal power plants [*Albertsson et al*., 2003].

Finally, chemical and mechanical interactions between pore fluids and rock may cause important modifications to the geometry of the pore space. Such interactions will undoubtedly influence both the strength and the transport properties of the rocks. Long-term experiments with reactive pore fluids are desirable in order to investigate the modifications of pore space induced by metamorphic reactions coupled with deformation [*Heap et al*., 2011].

5. Conclusions

New porosity and mechanical data obtained on basalts deformed at a constant strain rate of $10^{-5}\,s^{-1}$ and a confining pressure up to 130 MPa, pore pressure up to 30 MPa, and temperatures from 600°C to 1050°C are the first experimental studies of basalt porosity under brittle and ductile deformation mode at oceanic crustal conditions.

Mechanical and microstructural observations at $10^{-5}\,s^{-1}$ show that

1. The basalt was brittle and dilatant up to 800°C.
2. At higher temperatures the deformation mode became macroscopically ductile; i.e., deformation became distributed throughout the sample, while the basalt was compacting.
3. The new measurements suggest that the brittle to ductile transition may be considered as a limit of permeability in the oceanic crust. Therefore, the BDT may be an indicator of the maximum depth and temperature for the circulation of hydrothermal fluids. Extrapolation of these results to the Iceland oceanic crust conditions predicts that hydrothermal fluids might circulate, at least transiently, through the basaltic crust with thermal gradient of approximately 100°C/km down to 4 to 6 km depth.

Acknowledgments
We thank R. Lüchinger for thin sections preparation. We acknowledge R. Bakker for his help in the laboratory. M.V. and J.-P.B. thank the ETH for support; B.G. and D.M. thanks Geosciences Montpellier for support. In section 9, Figures 2 and 3 are the processed data. Raw data can be requested from marie.violay@erdw.ethz.ch. Mike Heap and an anonymous reviewer are thanked for their constructive comments that improved significantly our presentation.

The Editor thanks Michael Heap and an anonymous reviewer for their assistance in evaluating this paper.

References

Albertsson, A., J. O. Bjarnason, T. Gunnarsson, C. Ballzus, and K. Ingason (2003), The Iceland Deep Drilling Project: Fluid handling evaluation and utilization, in *Proceedings of the International Geothermal Conference IGC-2003 Reykjavik*, September 2003, Session 623–30.

Asmundsson, R., et al. (2014), High temperature instruments and methods developed for supercritical geothermal reservoir characterisation and exploitation—The Hiti Project, *Geothermics*, *49*, 90–98.

Bernabé, Y., W. F. Brace, and B. Evans (1982), Permeability, porosity and pore geometry of hot pressed calcite, *Mech. Mater.*, *1*, 173–183.

Chen, Y., and W. J. Morgan (1990), A non-linear rheology model for mid-ocean ridge axis topography, *J. Geophys. Res.*, *88*, 4183–4214, doi:10.1029/JB088iB05p04183.

De Paola, N., D. R. Faulkner, and C. Collettini (2009), Brittle versus ductile deformation as the main control properties of low-porosity anhydrite rocks, *J. Geophys. Res.*, *114*, B06211, doi:10.1029/2008JB005967.

Driesner, T., and S. Geiger (2007), Numerical simulation of multiphase fluid flow in hydrothermal systems, in *Fluid-Fluid Interactions*, *Rev. Mineral. Geochem.*, vol. 65, edited by A. Liebscher and C. A. Heinrich, pp. 187–212, Mineralog. Soc. of Am.

Fischer, G. J., and M. S. Paterson (1989), Dilatancy during rock deformation at high temperatures and pressures, *J. Geophys. Res.*, *94*(B12), 17,607–17,617, doi:10.1029/JB094iB12p17607.

Fischer, G. J., and M. S. Paterson (1992), The determination of permeability and storage capacity: Pore pressure oscillation method, in *Fault Mechanics and Transport Properties of Rocks*, *Int. Geophys. Ser.*, vol. 51, edited by B. Evans and T.-F. Wong, pp. 187–212, San Diego, Calif.

Fontaine, F. J., M. Rabinowicz, and J. Boulègue (2001), Permeability changes due to mineral diagenesis in fractured crust: Implications for hydrothermal circulation at mid-ocean ridges, *Earth Planet. Sci. Lett.*, *184*, 407–425.

Fontaine, F. J., M. Cannat, and J. Escartin (2008), Hydrothermal circulation at slow-spreading mid-ocean ridges: The role of long-axis variations in axial lithospheric thickness, *Geology*, *36*, 759–762, doi:10.1130/G24885A.1.

Fournier, R. O. (1999), Hydrothermal processes related to movement of fluid from plastic into brittle rock in the magmatic-epithermal environment, *Econ. Geol.*, *94*, 1193–1211.

Fridleifsson, G. O., and W. A. Elders (2005), The Iceland Deep Drilling Project: A search for deep unconventional geothermal resources, *Geothermics*, *34*, 269–285.

Friðleifsson, G. Ó., W. A. Elders, and A. Albertsson (2014), The concept of the Iceland Deep Drilling Project, *Geothermics*, *49*, 2–8, doi:10.1016/j.geothermics.2013.03.004.

Frost, H. J., and M. F. Ashby (1982), *Deformation-Mechanism Maps*, Pergamon, Oxford.

Hayba, D. O., and S. E. Ingebritsen (1997), Multiphase groundwater flow near cooling plutons, *J. Geophys. Res.*, *102*, 12,235–12,252, doi:10.1029/97JB00552.

Heap, M. J., P. Baud, P. G. Meredith, S. Vinciguerra, A. F. Bell, and I. G. Main (2011), Brittle creep in basalt: Implications for time-dependent volcano deformation, *Earth Planet. Sci. Lett.*, *307*, 71–82.

Ingebritsen, S. E., and C. E. Manning (2010), Permeability of the continental crust: Dynamic variations inferred from seismicity and metamorphism, *Geofluids*, *10*, 193–205 (Reprinted in Yardley, B., Manning, C., and Garven, G., eds., 2011, Frontiers in Geofluids: Chichester, U. K., Wiley-Blackwell, p. 193–205.).

Johnson, H. P., K. Becker, and R. Von Herzen (1993), Near-axis heat flow measurements on the northern Juan De Fuca Ridge: Implications for fluid circulation in oceanic crust, *Geophys. Res. Lett.*, *20*(17), 1875–1878, doi:10.1029/93GL00734.

Macdonald, K. C. (1982), Mid-ocean ridges: Fine scale tectonic, volcanic and hydrothermal processes within the plate boundary zone, *Ann. Rev. Earth Planet. Sci.*, *10*, 155–190.

Mills, R. A., and H. Elderfield (1995), Rare earth element geochemistry of hydrothermal deposits from the active TAG Mound, 26°N Mid-Atlantic Ridge, *Geochim. Cosmochim. Acta*, *59*, 3511–3524.

Mitchell, T., and D. R. Faulkner (2008), Experimental measurements of permeability evolution during triaxial compression of initially intact crystalline rocks and implications for fluid flow in fault zones, *J. Geophys. Res.*, *113*, B11412, doi:10.1029/2008JB005588.

Morgan, W. J., and Y. Chen (1993), Dependence of ridge axis morphology on magma supply and spreading rate, *Nature*, *364*, 706–708.

Nelson, C., and D. Giles (1985), Hydrothermal eruption mechanisms and hot spring gold deposits, *Econ. Geol.*, *80*(6), 1633–1639, doi:10.2113/gsecongeo.80.6.1633.

Palmason, G. (1974), Heat flow and hydrothermal activity in Iceland, in *Geodynamics of Iceland and the North Atlantic Area*, edited by L. Kristjansson, pp. 297–306, D. Reidel, Dordrecht, Netherlands.

Paterson, M. S., and T.-F. Wong (2005), Experimental rock deformation - The brittle field, 2nd ed., *348* pp., Springer, New York.

Peach, C. J., and C. J. Spiers (1996), Influence of crystal plastic deformation on dilatancy and permeability development in synthetic salt rock, *Tectonophysics*, *256*, 101–128.

Rojstaczer, S. A., S. E. Ingebritsen, and D. O. Hayba (2008), Permeability of continental crust influenced by internal and external forcing, *Geofluids*, *8*, 128–139.

Siddiqi, G., B. Evans, G. Dresen, and D. Freund (1997), Effect of semibrittle deformation on transport properties of calcite rocks, *J. Geophys. Res.*, *102*, 14,765–14,778, doi:10.1029/97JB01038.

Sleep, N. H., and B. R. Rosendahl (1979), Topography and tectonics of mid-oceanic ridge axes, *J. Geophys. Res.*, *84*, 6831–6839.

Stein, C., and S. Stein (1994), Constraints on hydrothermal heat flux through the oceanic lithosphere from global heat flow, *J. Geophys. Res.*, *99*, 3081–3095, doi:10.1029/93JB02222.

Violay, M. E. S., B. Gibert, D. Mainprice, B. Evans, J.-M. Dautria, P. Azais, and P. Pézard (2012), An experimental study of the brittle-ductile transition of basalt at oceanic crust pressure and temperature conditions, *J. Geophys. Res.*, *117*, B03213, doi:10.1029/2011JB008884.

Weis, J. P., T. Driesner, and C. A. Heinrich (2012), Porphyry-copper ore shells form at stable pressure-temperature fronts within dynamic fluid plumes, *Science*, *338*, 1613–1616.

Zoback, M., and J. Byerlee (1975), The effect of microcrack dilatancy on the permeability of Westerly Granite, *J. Geophys. Res.*, *80*, 752–755, doi:10.1029/JC080i015p01975.

Zhu, W., and T. F. Wong (1997), The transition from brittle faulting to cataclastic flow: Permeability evolution, *J. Geophys. Res.*, *102*(B2), 3027–3041, doi:10.1029/96JB03282.

Zhang, S., S. Cox, and M. Paterson (1994), The influence of room temperature deformation on porosity and permeability in calcite aggregates, *J. Geophys. Res.*, *99*, 15,761–15, 775, doi:10.1029/94JB00647.